Mechanical Systems and Signal Processing 184 (2023) 109422

Contents lists available at ScienceDirect

Mechanical Systems and Signal Processing

journal homepage: www.elsevier.com/locate/ymssp

Data-driven simultaneous identification of the 6DOF dynamic model and wave load for a ship in waves

Zhengru Ren [a,b], Xu Han [b], Xingji Yu [c,*], Roger Skjetne [b], Bernt Johan Leira [b], Svein Sævik [b], Man Zhu [d]

[a] Institute for Ocean Engineering, Shenzhen International Graduate School, Tsinghua University, Tsinghua Campus, University Town, Shenzhen 518055, China

[b] Centre for Research-based Innovation on Marine Operations (SFI MOVE), Department of Marine Technology, Norwegian University of Science and Technology (NTNU), NO-7491 Trondheim, Norway

[c] Department of Energy and Process Engineering, NTNU, NO-7491 Trondheim, Norway

[d] Intelligent Transportation Systems Research Center, Wuhan University of Technology, China

ARTICLE INFO

Communicated by J.E. Mottershead

Keywords:
Model identification
Data-driven method
Wave load estimation
Motion prediction
Sparse regression

ABSTRACT

In marine operations, the performance of model-based automatic control design and decision support systems highly relies on the accuracy of the representative mathematical models. Model fidelity can be crucial for safe voyages and offshore operations. This paper proposes a data-driven parametric model identification of a ship with 6 degrees of freedom (6DOF) exposed to waves using sparse regression according to the vessel motion measurements. The features of the complex ship dynamics are extracted and expressed as a linear combination of several functions. Thruster inputs and environmental loads are considered. The hydrodynamic coefficients and wave-induced loads are simultaneously estimated. Unlike earlier studies using a limited number of unknown functions, a library of abundant candidate functions is applied to fully consider the coupling effects among all DOFs. The benefit of the proposed method is that it does not require the exact construction of the library functions. Based on the estimated model, short-term motion prediction is achievable. The algorithm is verified through experiments. The method can be extended to other types of floating structures.

1. Introduction

Ship model identification has been an important topic for decades. A mathematical model is established to represent the ship dynamics based on the measured data. Over the past decades, technical advances in marine operations have gradually increased the level of autonomy, enhanced operational limitations, reduce operation risks, and helped avoid vital failures and hazards. The model fidelity plays an essential role in potential performance. Moreover, more precise models are expected to fulfill the state-of-the-art requirements of increasingly accurate simulations and various model-based algorithms, such as dynamic analysis [1], visualization, digitalization [2], short-term response prediction, operation planning [3], and decision support [4]. Therefore, the ship model identification continues to be of high practical value.

A ship is normally assumed to be a rigid body with a lumped mass. The values of hydrodynamic parameters are affected by many factors such as the hull geometry, wave conditions, and vessel loading conditions. A ship model is subject to high complexity,

* Corresponding author.
E-mail addresses: zhengru.ren@sz.tsinghua.edu.cn (Z. Ren), xu.han@ntnu.no (X. Han), xingji.yu@ntnu.no (X. Yu), roger.skjetne@ntnu.no (R. Skjetne), bernt.leira@ntnu.no (B.J. Leira), svein.savik@ntnu.no (S. Sævik), man.zhu.393@whut.edu.cn (M. Zhu).

https://doi.org/10.1016/j.ymssp.2022.109422
Received 16 June 2021; Accepted 7 June 2022

nonlinearity, and uncertainty. The identification problem is simplified into the concerning degrees of freedom (DOFs), starting the analysis in terms of the simplest 1DOF scenarios, such as the yaw motion of Nomoto model [5] and the roll dynamics [6,7]. A two-dimensional application is the identification of the steering dynamics for a surface vehicle, including the surge and yaw motions [8]. In addition, the 3DOF ship maneuvering model in the horizontal plane, including surge, sway, and yaw, is especially useful for modeling voyages and slow-speed stationkeeping operations [5,6,9–14,14–18]. Increasing attention has been paid to model the nonlinearities. The involvement of nonlinear damping slightly improves the performance of dynamic positioning systems [19]. In contrast to the operations in the horizontal plane, all 6 DOFs are crucial for the safety of on-site marine operations, e.g., lifting and pipe laying. To the best of the authors' knowledge, the 6DOF model identification of a ship remains lacking. The complexities mainly arise from the coupling effects among 6 DOFs and environmental uncertainties.

Model identification is categorized into parametric and nonparametric approaches depending on the existence of explicit mathematical expressions. A mathematical expression is assumed to be available a priori in the parametric methods. Many theories have been developed to convert complex physical ship dynamics into an elegant mathematical equation using few coefficients. Hence, the core problem of ship model identification is to find these coefficients to minimize the error between the estimated dynamics and the measured data. Potential candidates are adaptive tracking control [5,9] regression-based approaches (e.g., genetic algorithm [10,20] and support vector regression [6,14,21]), and Kalman filters [12,16]. In an adaptive control design, the weighting vector is simultaneously updated when the control law minimizes the tracking error. The ship dynamics are estimated online, and the control input cancels the unknown term in the error dynamics to ensure the convergence of the tracking error. However, the update of the weighting vector is only related to the present time instant, where the historical data are accumulated in the states. An accurate identification of the unknown coefficients also requires the persistency of excitation conditions to hold, i.e., one cannot identify the parameters of the model that are not excited through the inputs to the model. For a system where there are many more parametric functions than DOFs, the model identified from adaptive control or an extended Kalman filter (EKF) gives a locally optimal and consequently a poor motion prediction. Regression-based and EKF-based approaches also require an assumed explicit mathematical expression. Regression-based approaches typically apply the minimum least square [22] and maximum likelihood principles [23]. The overfitting problem caused by measurement noise limits the applications of the regression-based approach.

Due to the absence of physical meaning, input–output models are considered nonparametric or black-box models. Using abundant data, artificial neural networks are trained to approximate the vessel dynamics [11,24]. The training process can be accomplished through online neural adaptive tracking [13] and offline using the measured data [25]. The major drawbacks of neural networks are a lack of physical meanings and inferior extrapolation capacity. The performance of the trained model greatly depends on the adequacy of measurement data. In addition, the modeling of stochastic environmental loads, such as waves and wind, is challenging. Hence, motion prediction based on the identified model can be problematic.

There are three methods to verify the identification algorithms. The most commonly used approach is numerical simulation generated by the relevant selected codes in a known form [5,6,10,11,13–15]. However, a critical question is to what degree the equations in the simulations will precisely represent the ship dynamics. As a mitigating measure, some limited research has been based on validating the model equations through experimental model tests [9,17,26] and sea trials [12]. Although the experiments and sea trials are time-consuming and expensive, they provide higher credibility of the identification approach. For applications in the horizontal plane, zigzag tests, turning circle tests, and free runs are widely applied.

An obvious shortcoming of the aforementioned research work is the lack of consideration of wave-induced motions. Although wave-induced motions have minor effects on maneuvering in the horizontal plane, they are critical to all types of in situ marine operations using floating vessels, such as lifting operations. Wave load estimation and prediction have attracted increasing research interest in relation to high-precision marine operations [27]. Wave-induced motions are the fundamental problem to overcome for an onboard heave-compensation system. Various methods have been developed to calculate the wave loads on a vessel, such as the linear and nonlinear strip theories [28], unified slender body theory [29], Green's function method [30], and Rankine source method [31].

Sparse regression has been applied to the reduced-order modeling of nonlinear dynamic systems, such as discovering the governing equations of vortex-induced vibration [32] and directional wave spectrum [33,34]. It removes the number of components in the optimal solution and can reduce the estimation variance and improve the robustness by inducing sparsity in the parameters.

In this paper, a data-driven approach is proposed to identify a 6DOF ship model exposed to irregular waves based on motion measurements. The coupled hydrodynamic coefficients and wave information are estimated. The main contributions are listed as follows.

- To the best of our knowledge, onboard 6DOF white-box ship model identification based on vessel motions is studied for the first time;
- Complex and high-order fluid–structure interaction effects are considered in the proposed linear model, such as the linear and nonlinear hydrodynamics, the influence of directional wave spectrum, and thruster inputs;
- Sparse regression is firstly applied to ship model identification. Unlike the typical approaches, the selection of candidate functions can be more flexible;
- The prediction of short-term wave loads is achievable by using the identified model.

The remainder of the paper is organized as follows. The ship model and identification problem are formulated in Section 2. In Section 3, the model identification algorithm is proposed. In accordance with the identification results, wave load estimation and short-term motion prediction are achievable. The results of an experimental verification using a moored drillship model are presented and discussed in Section 4. The paper is summarized in Section 5.

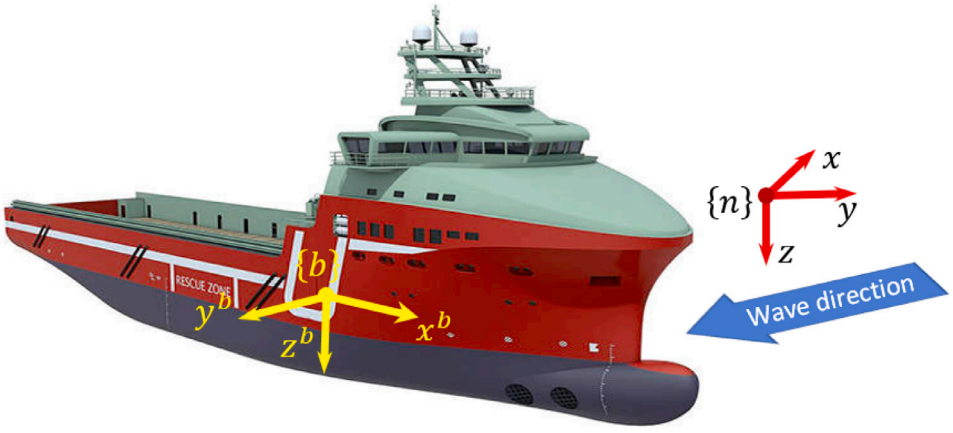

Fig. 1. Coordinate systems of a floating ship.

2. Problem formulation

2.1. System modeling

For a ship, two right-hand reference frames are defined as follows: see Fig. 1.

- North-east-down (NED) coordinate system $\{n\}$: The origin is placed at the free-water surface with the x-, y-, and z-axes pointing to the north, east, and downward, respectively.
- Body-fixed reference frame $\{b\}$: The origin is located at the ship mass center. The x^b-axis stays in the ship longitudinal axis and points to the bow, the y^b-axis points to the starboard, and the z^b-axis points downwards. Euler angles are defined as the rotations about the x-, y-, and z-axes, i.e., roll (ϕ), pitch (θ), and yaw (ψ), respectively. The Euler angle vector is $\Theta = [\phi, \theta, \psi]^\top$.

The ship is modeled as a rigid body where the local flexibility is neglected. The wave direction β_{wave} is defined as the direction from which the waves are approaching. Similar definitions are assigned to the current and wind directions, i.e., β_{cur} and β_{wind}. A widely used 6DOF ship model is given by

$$\dot{\eta} = J(\Theta)\nu, \tag{1a}$$

$$(M_{RB} + M_A)\dot{\nu} + C(\nu)\nu + D(\nu)\nu + g(\eta) = \tau_{thr} + \tau_{moor} + \tau_{wind} + \tau_{cur} + \tau_{wave1} + \tau_{wave2}, \tag{1b}$$

where $\eta = [x, y, z, \phi, \theta, \psi]^\top$ denotes the translational displacement and rotation in coordinate system $\{n\}$, $\nu = [u, v, w, p, q, r]^\top$ is the vector of translational and rotational velocity in coordinate system $\{b\}$, $J(\Theta)$ is the rotation matrix from $\{b\}$ to $\{n\}$, $g(\eta) \approx G\eta$ is the restoring force, M_{RB}, M_A, $C(\nu)$, and $D(\nu) \in \mathbb{R}^{6\times6}$ are the matrices of the rigid-body mass, added mass, Coriolis matrix, and damping coefficients, respectively. The external loads τ_{moor}, τ_{cur}, and τ_{wind} denote vectors of force and torque acting on the ship caused by the mooring system, current, and wind, respectively. The thruster input τ_{thr} is known and used as prior information. In addition, τ_{wave1} and τ_{wave2} are the first- and second-order wave-induced loads. Eqs. (1a) and (1b) are the kinematic and kinetic equations, respectively. The complex hydrodynamic loads acting on the ship are simplified as the superposition of several parts. The hydrodynamic radiation force is modeled by the terms $M_A\dot{\nu}$ and $D(\nu)\nu$, which are assumed to be constant in a specific sea state. τ_{moor} and τ_{thr} are optional and depend on the vessel characteristics.

The current- and wind-induced loads (τ_{cur} and τ_{wind}), and the second-order wave drift loads (τ_{wave2}), are considered constant if we assume that the speeds and headings of the wind and current, remain steady and constant during a measurement period. If the rotational motions are small, the exposed area is assumed to remain the same during a measurement period. Thus, the resulting wind loads are assumed to be constant.

The mooring system introduces additional damping and restoring terms to the system dynamics [35], i.e.,

$$\tau_{moor} = -G_{moor}(\eta - \bar{\eta}) - D_{moor}\nu, \tag{2}$$

where $\bar{\eta}$ denotes the mean position and orientation of the mooring system at rest, and G_{moor} and D_{moor} are the generalized restoring and damping matrices of the mooring system, respectively.

According to linear wave theory, the wave spectrum is discretized into many sinusoidal wave components, where the corresponding first-order wave-induced loads τ_{wave1} acting on the ship are affected by the wave force response amplitude operator (RAO). The water surface elevation is modeled as a superposition of n_w wave components. Hence, the wave-excitation force or torque acting in

the ith DOF is given by

$$\begin{aligned}\tau_{wave1,i} &= \sum_{j}^{n_w} \Phi_{ij}(\omega_j,\beta_j)A_{w,j}\sin(\omega_j t + k_{xj}x + k_{yj}y + \varphi_j + \epsilon_j)\\ &= \sum_{j}^{n_w} k_{cij}\sin(\omega_j t) + \sum_{j}^{n_w} k_{sij}\cos(\omega_j t),\end{aligned} \tag{3}$$

where subscript j is the index of the corresponding wave component, n_w is the number of wave components, Φ is the wave force RAO, A_w is the amplitude of the wave component, $k_{cij} = \Phi_{ij}A_{w,j}\cos(k_{xj}x + k_{yj}y + \varphi_j + \epsilon_j)$ and $k_{sij} = \Phi_{ij}A_{w,j}\sin(k_{xj}x + k_{yj}y + \varphi_j + \epsilon_j)$, and ω, β, φ, ϵ, k_x and k_y are the wave frequency, wave heading, RAO phase, random phase, and wave numbers in the x- and y-directions, respectively.

2.2. Problem statement

Substituting Eqs. (2) and (3) into the 6DOF kinetic Eq. (1b) yields

$$\begin{aligned}\dot{\nu} \;=\;& M^{-1}[-C(\nu)\nu - (D(\nu) + D_{moor})\nu - (G + G_{moor})\eta] && \text{(I)}\\ &+M^{-1}\tau_{thr}(t) && \text{(II)}\\ &+M^{-1}(\tau_{wind} + \tau_{cur} + \tau_{wave2} + G_{moor}\bar{\eta}) && \text{(III)}\\ &+M^{-1}K_c S_\omega(t) + M^{-1}K_s C_\omega(t), && \text{(IV)}\end{aligned} \tag{4}$$

where $M = M_{RB} + M_A$ is the total mass matrix, $S_\omega(t) = [\sin(\omega_1 t),\ldots,\sin(\omega_{n_\omega} t)]^\top$ and $C_\omega(t) = [\cos(\omega_1 t),\ldots,\cos(\omega_{n_\omega} t)]^\top$ contain the sine and cosine functions of a number of discretized frequencies,

$$K_c = \begin{bmatrix} k_{c11} & k_{c12} & \cdots & k_{c1n_\omega}\\ k_{c21} & k_{c22} & \cdots & k_{c2n_\omega}\\ \vdots & \vdots & \ddots & \vdots\\ k_{c61} & k_{c62} & \cdots & k_{c6n_\omega}\end{bmatrix}, \text{ and } K_s = \begin{bmatrix} k_{s11} & k_{s12} & \cdots & k_{s1n_\omega}\\ k_{s21} & k_{s22} & \cdots & k_{s2n_\omega}\\ \vdots & \vdots & \ddots & \vdots\\ k_{s61} & k_{s62} & \cdots & k_{s6n_\omega}\end{bmatrix}.$$

According to the independent variables, Eq. (4) is categorized into four parts as labeled:

(I) The motion-dependent term: the information of Coriolis effects, hydrodynamic effects, damping force, and restoring force;
(II) The time-varying and known term: thruster input τ_{thr};
(III) The constant unknown term: wind-, current-, second-order wave-, and mooring-system-induced force and torque;
(IV) The harmonic terms: wave-induced loads that are functions of time.

A stationkeeping scenario is considered. Several assumptions are adopted.

- The directional wave spectrum remains steady during the measurement period, and the ship stays at a constant position (x, y) with a constant heading ψ. Hence, k_{cij} and k_{sij} are constant unknown parameters.
- The thruster inputs are assumed to be known.
- τ_{wave2}, and $G_{moor}\bar{\eta}$ are considered constant and unknown. The effects of wind and current (τ_{wind} and τ_{cur}) are assumed to be a part of the constant load.
- We assume that the coefficients in (4) are constant for a given sea state.

When η, ν, and $\dot{\nu}$ are known, it is possible to identify the unknown coefficients based on the aforementioned simplifications and assumptions. In most former studies, the mass matrix M is assumed to be diagonal, which results in decoupled ship dynamics, i.e., the dynamics of each DOF are only affected by a small portion of relevant terms. However, the expression for the model in each DOF is more complicated if the mass matrix M is not exactly diagonal due to the added mass matrix M_A. The 6DOF coupling effects are considered. If the wave loads are functions of time and wave frequencies as shown in (3), the wave loads in the short term can be predicted. With the identified ship model, the short-term motion is also predictable.

The ship motions can be directly measured by sensors or estimated through model-based or model-free observers. Hereafter, we consider that all translational displacement, rotations, and their corresponding velocities and accelerations are well estimated. This paper aims to identify the parametric 6DOF ship model and wave load model in (4) based on the measured vessel motion data.

3. Model identification

3.1. Sparse regression of the ship model

Categorizing Eq. (4) into two parts and rewriting it into affine form yields

$$\dot{\nu} = \zeta^\top \varphi(\eta,\nu,\tau_{thr}) + \zeta_w^\top \varphi_w(t), \tag{5}$$

where

$$\zeta^{\top}\varphi(\eta,\nu,\tau_{thr}) = M^{-1}[-C(\nu)\nu - (D(\nu)+D_{moor})\nu - (G+G_{moor})\eta + \tau_{thr}(t)],$$

$$\zeta_w^{\top}\varphi_w(t) = M^{-1}(b + K_c S_\omega(t) + M^{-1}K_s C_\omega(t)),$$

$b = \tau_{wind} + \tau_{cur} + \tau_{wave2} + G_{moor}\bar{\eta}$, $\varphi \in \mathbb{R}^{n_1}$ and $\varphi_w \in \mathbb{R}^{n_2}$ are two libraries of the pre-designed candidate functions, n_1 and n_2 are the numbers of functions in the libraries, $\zeta \in \mathbb{R}^{n_1 \times n_{dof}}$ and $\zeta_{w,ij} \in \mathbb{R}^{n_2 \times n_{dof}}$ are the matrices containing the unknown coefficients to be identified, and n_{dof} is the number of DOFs to be identified. For each DOF, there is a column in ζ and ζ_w. Hereafter, $n_{dof} = 6$.

The first term $\zeta^{\top}\varphi$ is time-invariant and contains the state-dependent terms and known time-varying thruster load. The second term $\zeta_w^{\top}\varphi_w$ is sea-state-dependent and time-varying, and it denotes the first-order wave-induced loads and unknown constant loads, where φ_w contains functions of t. Specifically, the dimensionless wave-induced loads are defined as

$$\bar{\tau}_{wave}(t) = M^{-1}\tau_{wave2}(t). \tag{6}$$

From Eq. (3), the coefficients in ζ_w are affected by the incoming wave direction, wave frequency, wave height, and relative phase.

In earlier studies where regression methods are applied, the concerned dynamics are assumed to be a linear superposition of several known candidate functions, and n_1 and n_2 are small. However, the nonlinear dynamics are not accurately expressed for some conditions. Instead of a small portion of unknowns components, we select many candidate functions considering the coupling effects. The regression problem becomes sparse regression if the coefficients of only a small fraction of these terms are nonzero. The benefit of this method is that it does not require the exact construction of the library functions.

For a specific time instant t_k, we have

$$\dot{\nu}^{\top}(t_k) = \zeta^{\top}\varphi(t_k) + \zeta_w^{\top}\varphi_w(t_k) = \begin{bmatrix}\varphi^{\top}(t_k) & \varphi_w^{\top}(t_k)\end{bmatrix}\begin{bmatrix}\zeta \\ \zeta_w\end{bmatrix}. \tag{7}$$

Along a measurement period ($k = 1, \ldots, n_t$), the matrix form of (7) becomes

$$\dot{V} = \boldsymbol{\Phi}(\eta,\nu,\tau_{thr})\zeta + \boldsymbol{\Phi}_w(t)\zeta_w, \tag{8}$$

where $\dot{V} = [\dot{\nu}(t_1), \ldots, \dot{\nu}(t_{n_t})]^{\top} \in \mathbb{R}^{n_t \times n_{dof}}$, $\boldsymbol{\Phi} = [\varphi(t_1), \ldots, \varphi(t_{n_t})]^{\top} \in \mathbb{R}^{n_t \times n_1}$, and $\boldsymbol{\Phi}_w = [\varphi_w(t_1), \ldots, \varphi_w(t_{n_t})]^{\top} \in \mathbb{R}^{n_t \times n_2}$. Each row of $\boldsymbol{\Phi}$ and $\boldsymbol{\Phi}_w$ contains the values of the selected candidate functions at a time instant, and each column denotes the value of a specific candidate function at all time instants.

The values of regression coefficients ζ and ζ_w are the solution of the following LASSO (least absolute shrinkage and selection operator) problem [36,37]

$$\min_{\zeta,\zeta_w}\left\{\|\dot{V} - \boldsymbol{\Phi}(\eta,\nu,\tau_{thr})\zeta - \boldsymbol{\Phi}_w(t)\zeta_w\|_2^2 + \lambda_1\|\zeta\|_1 + \lambda_2\|\zeta_w\|_1\right\}, \tag{9}$$

where λ_1 and λ_2 are the hyperparameters to be tuned. $\|\zeta\|_1$ and $\|\zeta_w\|_1$ are penalties to ensure the sparsity. The least square regression results in nonzero values of most elements in ζ and ζ_w. Hence, L1 norms are added to increase the sparsity in the results. The selection of discretized wave frequencies ω_j ($j = 1, \ldots, n_\omega$) should also be tuned.

A convenient method to increase the amount of training data is to collect motion data in the same sea state with different headings. The collected data can be fused to improve the estimation accuracy in case some coupling effects are not considerably excited for specific wave headings, e.g., the sway motion in a head sea. $\boldsymbol{\Phi}\zeta$ is assumed to be identical, whereas ζ_w varies with ship headings. Suppose that there are a total number n_{exp} of measurement periods; then, the fusion form of Eq. (9) is given by

$$\min_{\zeta,\zeta_{w,m}}\left\{\sum_m^{n_{exp}}\|\dot{V}_m - \boldsymbol{\Phi}(\eta,\nu,\tau_{thr})\zeta + \boldsymbol{\Phi}_w(t)\zeta_{w,m}\|_2^2 + \lambda_1\|\zeta\|_1 + \lambda_2\sum_m\|\zeta_{w,m}\|_1\right\}, \tag{10}$$

where subscript m denotes the index of the sampling period.

Since the dynamics in Eq. (5) are dimensionless, the coefficients of meaningful terms are expected to be within a similar order of magnitude. After programming, the value of a coefficient in ζ or $\zeta_{w,m}$ should be set to zero if its absolute value is less than a small positive constant threshold tolerance ε_{ship} and ε_{wave}, respectively. Besides, if the norm of all coefficients related to a specific frequency ω_j is smaller than a preset small constant threshold tolerance, $\varepsilon_{wave,total}$, all coefficients are neglected. Normally, $\varepsilon_{wave,total} \gg \varepsilon_{wave}$. By controlling the values of ε_{ship}, ε_{wave}, and $\varepsilon_{wave,total}$, it is possible to control the number of active terms in the library. The algorithm is summarized in Algorithm 1 below.

The proposed algorithm can only calculate the coupled coefficients. For example, it is impossible to extract the hydrodynamic parameters of the mass matrix. Another example is that the RAO, wave amplitude, and wave phase cannot be separated, since they are coupled in parameters k_{sij} and k_{cij}. Furthermore, the mass M_{RB} and added mass M_A are coupled in the dynamics and consequently impossible to individually identify.

To enhance the computational efficiency, optimization can be separately conducted for each DOF. If so, V_m is a column vector.

Algorithm 1: Remove candidate functions with minor effects.

Inputs: ζ, $\zeta_{w,m}$
Parameters: ε_{ship}, ε_{wave}, $\varepsilon_{wave,total}$
for *All elements in* ζ **do**
  if $\zeta < \varepsilon_{ship}$ **then**
    $\zeta = 0$
  end
end
for $m = 1 : n_\omega$ **do**
  if $\zeta_{w,m} < \varepsilon_{wave,total}$ **then**
    $\zeta_{w,m} = 0$
  else
    for *All elements in* ζ **do**
      if $\zeta_{w,m} < \varepsilon_{wave}$ **then**
        $\zeta_{w,m} = 0$
      end
    end
  end
end

3.2. Motion prediction

According to the identified model, it is possible to predict its short-term motion for a ship without the thruster input. The states at time t_k can be obtained by integration based on (5) and (1a) using the current states at time instant t_0, i.e.,

$$\begin{bmatrix}\hat{\eta}\\ \hat{\nu}\end{bmatrix}(t_k|t_0) = \int_{t_0}^{t_k} \begin{bmatrix} J(\Theta)\nu(t) \\ \zeta^\top \varphi(t) + \zeta_w^\top \varphi_w(t)\end{bmatrix} dt. \tag{11}$$

When the control algorithm is explicit, it is possible to predict the motion and thruster input τ_{thr} recursively as a closed loop with time interval Δt; see Algorithm 2.

Algorithm 2: Motion prediction based on identified model

Inputs: $\hat{\eta}(t_0) = \eta(t_0)$, $\hat{\nu}(t_0) = \nu(t_0)$
for k **do**
  $\tau_{thr}(t_k) = \text{control law}(\hat{\eta}(t_k), \hat{\nu}(t_k))$
  $\begin{bmatrix}\hat{\eta}\\ \hat{\nu}\end{bmatrix}(t_{k+1}) = \begin{bmatrix}\hat{\eta}\\ \hat{\nu}\end{bmatrix}(t_k) + \begin{bmatrix} J(\hat{\Theta}(t_k))\hat{\nu}(t_k) \\ \zeta^\top \varphi(t_k) + \zeta_w^\top \varphi_w(t_k)\end{bmatrix}(t_{k+1} - t_k)$
end

3.3. Construction of candidate functions

The selection of candidate functions in the library is crucial to the identification performance. Different combinations should be tested in practical applications to determine the most efficient and accurate library. The libraries should be selected according to physical reasoning and convergence of fitting. We assume that the library is sufficiently rich and diverse to present the major ship dynamics. Since the sparse model is a reduced-order system, physical meanings for some candidate functions may not be guaranteed in a well-defined library.

In the simulations, the candidate functions were selected based on the knowledge of hydrodynamics and oceanography. The linear, quadratic, absolute, rotation, sine and cosine of wave frequency and time, and all their combinations are suitable candidates to be the basis functions in the library. Only the translational and rotational velocities ν contribute to the damping and Coriolis terms. The nonlinear dynamics $D(\nu)\nu$ are approximated by a Taylor series to be functions of ν. The wave-induced loads are affected by the vessel orientations, wave frequency, RAO, and relative direction between heading and incoming wave directions. The amount of required data increases with the growing complexity of the selected library, and $n_t \gg n_1 + n_2$.

Here, the libraries of candidate functions were selected to be

$$\varphi = \text{unique}([\eta^\top, \nu^\top, |\nu|^\top, \nu^\top \otimes \nu^\top, \nu^\top \otimes |\nu|^\top, \sin(\Theta^\top), \cos(\Theta^\top)]) \tag{12}$$

$$\varphi_w = \left[1, [1, \sin(\Theta^\top), \cos(\Theta^\top)] \otimes [\sin(\omega_1 t), \cos(\omega_1 t), \ldots, \sin(\omega_j t), \cos(\omega_j t), \ldots]\right] \tag{13}$$

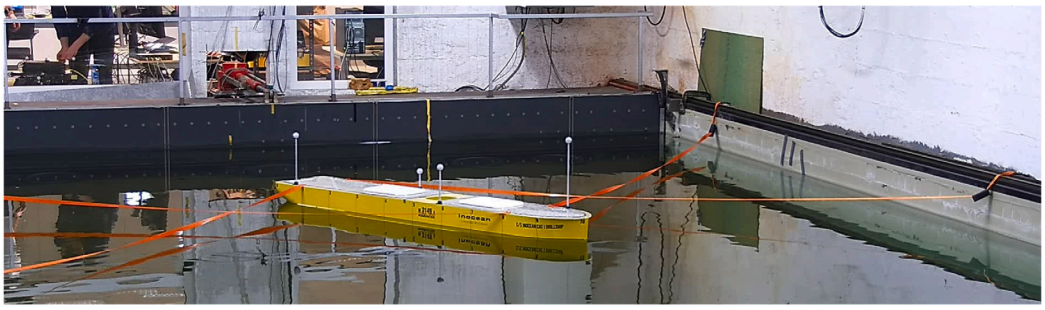

Fig. 2. Experimental setup in MCLab [38].

Table 1
The lengths of data collection periods in the experiments (unit: second).

T_p	β_{wave}					
	0 deg	30 deg	60 deg	90 deg	120 deg	150 deg
1.5 s	25	50	50	45	40	40

Table 2
Three groups of threshold tolerances in the simulations.

	esp1	esp2	esp3
ϵ_{ship}	0.005	0.001	0.0001
ϵ_{wave}	0.05	0.01	0.001
$\epsilon_{wave,total}$	0.005	0.001	0.0001

where $\otimes$ denotes the Kronecker product operator. Since uv and vu are identical, a unique operator is defined that removes the repeated combinations and outputs the unique components in a vector.

If τ_{wind} or τ_{cur} are assumed to be constant in a given measurement period, they are functions of wind and wave relative heading direction. Additional candidate functions of the discretized relative heading can be used to estimate the incoming wind and wave directions, such as $\sin(\psi-\beta_{cur,j})$, $\cos(\psi-\beta_{cur,j})$, $\sin(\psi-\beta_{wind,j})$, and $\cos(\psi-\beta_{wind,j})$. When the wind and current directions are known, the additional candidate functions are simplified to be $\sin(\psi-\beta_{cur})$, $\cos(\psi-\beta_{cur})$, $\sin(\psi-\beta_{wind})$, and $\cos(\psi-\beta_{wind})$.

4. Experiment

4.1. Experimental setup

Experiments were conducted in the Marine Cybernetics Laboratory (MCLab) at NTNU to verify the proposed algorithm [38]. A model drillship [39] was employed to verify the algorithm. The ship model has a length of 2.578 m, a breadth of 0.44 m, and a design draught of 0.133 m (see Fig. 2).

The vessel was stabilized by four wires at one side of a towing tank in the longitudinal direction. Regular waves were generated by a wave generator placed on the other side. In the towing tank, the incoming waves can only come from the x-axis. The vessel heading is changed to simulate different incoming wave directions. Since the wave-induced loads with symmetric incoming wave directions about the x^b-axis have an identical amplitude, the incoming wave direction was set to be 0, 30, 60, 90, 120, and 150 deg. The wave periods were set to 1.5 s. Each experiment took 100 s. To simulate a stationary sea state, only the motion data after the initial transition period were recorded. The lengths of the data collection periods are tabulated in Table 1. The last 10 s were used to verify the prediction.

The motion capture system was used to measure the motions with 1 mm accuracy. The sampling frequency was 100 Hz. The origin was set to be the mean position and orientation during the measurement. In the simulations, library Φ contained $n_1 = 416$ candidate functions. The relevant wave frequencies were selected to be 0.25 to 2.5 rad/s with an interval of 0.25 rad/s, which results in $n_2 = 810$ candidate functions in Φ_w. Three groups of threshold tolerances were used to evaluate their affects; see Table 2.

4.2. Results: Model fitting and prediction

After sparse regression and removing the minor components from the estimates, we tabulated the remaining candidate functions in Table 3. The calculation took about 5 min using a Core i7-4790 CPU 3.6 GHz. The 6DOF dynamics of the ship model are expressed by the addition of several functions.

One benefit of the proposed algorithm is that the selection of candidate functions is more flexible. We notice that only a few (less than 25 out of 416) of these functions are involved in the estimates. The unnecessary functions (391 out of 416) are removed.

Table 3
The components with major effects on the ship dynamics. The nonzero elements are marked by bullets.

$\dot{u}$	$\{\varepsilon_1\}$	$\{\varepsilon_2\}$	$\{\varepsilon_3\}$
$w\cos(\psi)$	•	•	•
$\cos(\theta)\sin(\psi)$		•	•
$\cos(\psi)\sin(\psi)$		•	•
$\cos(\psi)^2$		•	•
$p\cos(\phi)^2$	•	•	•
$p\cos(\psi)^2$	•	•	•
$\lvert p\rvert\sin(\psi)^2$	•	•	•
$\lvert r\rvert\cos(\phi)^2$			•
$\lvert q\rvert\cos(\phi)\cos(\psi)$	•	•	•
$\lvert p\rvert\cos(\psi)^2$	•	•	•

$\dot{q}$	$\{\varepsilon_1\}$	$\{\varepsilon_2\}$	$\{\varepsilon_3\}$
$\sin(\phi)$	•	•	•
$\sin(\theta)$	•	•	•
$r\sin(\psi)$	•	•	•
$w\cos(\psi)$	•	•	•
$\sin(\psi)^2$	•	•	•
$\cos(\theta)\sin(\psi)$	•	•	•
$\cos(\psi)\sin(\psi)$	•	•	•
$\cos(\psi)^2$		•	•
$p\cos(\phi)^2$			•
$p\cos(\psi)\cos(\theta)$	•	•	•
$\cos(\phi)^2\lvert w\rvert$	•	•	•
$\lvert r\rvert\cos(\psi)\cos(\theta)$	•	•	•

$\dot{r}$	$\{\varepsilon_1\}$	$\{\varepsilon_2\}$	$\{\varepsilon_3\}$
w	•	•	•
r	•	•	•
$\sin(\psi)^2$		•	•
$\cos(\psi)\sin(\psi)$	•	•	•
$p\sin(\psi)^2$	•	•	•
$q\cos(\theta)\sin(\psi)$	•	•	•
$p\cos(\phi)\cos(\psi)$	•	•	•
$q\cos(\theta)^2$	•	•	•
$\lvert q\rvert\cos(\phi)^2$	•	•	•
$\lvert p\rvert\cos(\phi)\cos(\psi)$			•
$\lvert r\rvert\cos(\psi)\cos(\theta)$	•	•	•

$\dot{v}$	$\{\varepsilon_1\}$	$\{\varepsilon_2\}$	$\{\varepsilon_3\}$
w	•	•	•
$p\lvert p\rvert$	•	•	•
$\sin(\phi)$	•	•	•
$w\sin(\psi)$	•	•	•
$q\cos(\psi)$	•	•	•
$\lvert p\rvert\cos(\psi)$	•	•	•
$\lvert q\rvert\cos(\psi)$		•	•
$\sin(\psi)^2$	•	•	•
$\cos(\psi)\sin(\psi)$	•	•	•
$\cos(\phi)\cos(\psi)$		•	•
$\cos(\psi)^2$	•	•	•
$v\cos(\phi)^2$	•	•	•
$\lvert w\rvert\sin(\psi)^2$	•	•	•
$\lvert r\rvert\sin(\psi)^2$	•	•	•
$\lvert q\rvert\cos(\phi)^2$	•	•	•
$\lvert p\rvert\cos(\theta)^2$	•	•	•
$\lvert q\rvert\cos(\psi)^2$	•	•	•
$\lvert r\rvert\cos(\psi)^2$	•	•	•

$\dot{w}$	$\{\varepsilon_1\}$	$\{\varepsilon_2\}$	$\{\varepsilon_3\}$
$\sin(\phi)$	•	•	•
$u\cos(\psi)$	•	•	•
$q\cos(\psi)$			•
$\lvert q\rvert\sin(\psi)$	•	•	•
$\lvert q\rvert\cos(\theta)$	•	•	•
$\sin(\psi)^2$		•	•
$\cos(\psi)\sin(\psi)$	•	•	•
$\cos(\psi)\cos(\theta)$		•	•
$\cos(\psi)^2$	•	•	•
$p\sin(\psi)^2$	•	•	•
$v\cos(\phi)\sin(\psi)$	•	•	•
$p\cos(\psi)\sin(\psi)$	•	•	•
$v\cos(\phi)^2$	•	•	•
$r\cos(\phi)\cos(\psi)$	•	•	•
$p\cos(\psi)\cos(\theta)$	•	•	•
$q\cos(\psi)\cos(\theta)$	•	•	•
$\lvert p\rvert\sin(\psi)^2$	•	•	•
$\lvert r\rvert\cos(\theta)^2$	•	•	•
$\lvert p\rvert\cos(\psi)^2$	•	•	•

$\dot{p}$	$\{\varepsilon_1\}$	$\{\varepsilon_2\}$	$\{\varepsilon_3\}$
u	•	•	•
q	•	•	•
p^2	•	•	•
$w\lvert p\rvert$	•	•	•
$p\lvert p\rvert$	•	•	•
$\sin(\phi)$	•	•	•
$q\cos(\psi)$	•	•	•
$\lvert w\rvert\sin(\psi)$	•	•	•
$\lvert r\rvert\cos(\theta)$	•	•	•
$\cos(\psi)\sin(\phi)$	•	•	•
$\cos(\phi)\sin(\theta)$	•	•	•
$\cos(\psi)\sin(\theta)$	•	•	•
$\cos(\phi)\sin(\psi)$	•	•	•
$\cos(\psi)\sin(\psi)$	•	•	•
$p\sin(\psi)^2$	•	•	•
$v\cos(\phi)\sin(\psi)$	•	•	•
$p\cos(\phi)^2$	•	•	•
$w\cos(\theta)^2$	•	•	•
$r\cos(\psi)\cos(\theta)$	•	•	•
$\lvert w\rvert\sin(\psi)^2$	•	•	•
$\lvert p\rvert\sin(\psi)^2$	•	•	•
$\cos(\phi)^2\lvert v\rvert$	•	•	•
$\cos(\phi)\cos(\psi)\lvert v\rvert$	•	•	•
$\lvert q\rvert\cos(\phi)\cos(\psi)$			•
$\lvert p\rvert\cos(\psi)^2$	•	•	•

The number of candidate functions increases with the reduction of the threshold. However, decreasing the thresholds by a factor of 5 and 50 in {esp2} and {esp3} only induces at most four additional candidate functions.

For each heading, the fitting of acceleration and 10-second velocity prediction are presented in Figs. 3–8. The origin $t = 0$ is at the end of the fitting and at the beginning of the prediction. The prediction was based on the estimated coefficients after removing the minor components.

The fitting was not significantly affected by removing the minor components, which shows that the major components well represented the system dynamics. Although the fitting was improved by reducing thresholds, the differences are mainly related to the motions with low amplitudes, e.g., the sway motion $\dot{v}$ in Fig. 3 when the ship is subjected to head seas and the surge motion $\dot{u}$ in Fig. 6 in beam seas. The best fitting performance was noticed in Figs. 4, 5, 7, and 8, since the motion in every DOF is better excited. The reflected waves from the tank wall affect the model as disturbances.

The predicted future motions in 10 s were satisfactory. The prediction had an identical tendency to the fitting. For motions with small amplitudes, some subtle high-frequency parts were neglected. In addition, the accumulated bias drifted the prediction away from the real value, which resulted in a growing prediction error over time. Employing a small threshold effectively reduced the error; however, this strategy included more minor candidate functions, which resulted in a risk of overfitting.

An applicable approach to increase the number of training data is to increase the measurement time in each measurement period. However, the computation time grows exponentially with the number of samples. The proposed algorithm can identify a proper model, but efforts are required to apply the proposed technique for real-time model estimation and motion prediction. According to the estimated hydrodynamic coefficients and wave model, the prediction of wave loads is also possible.

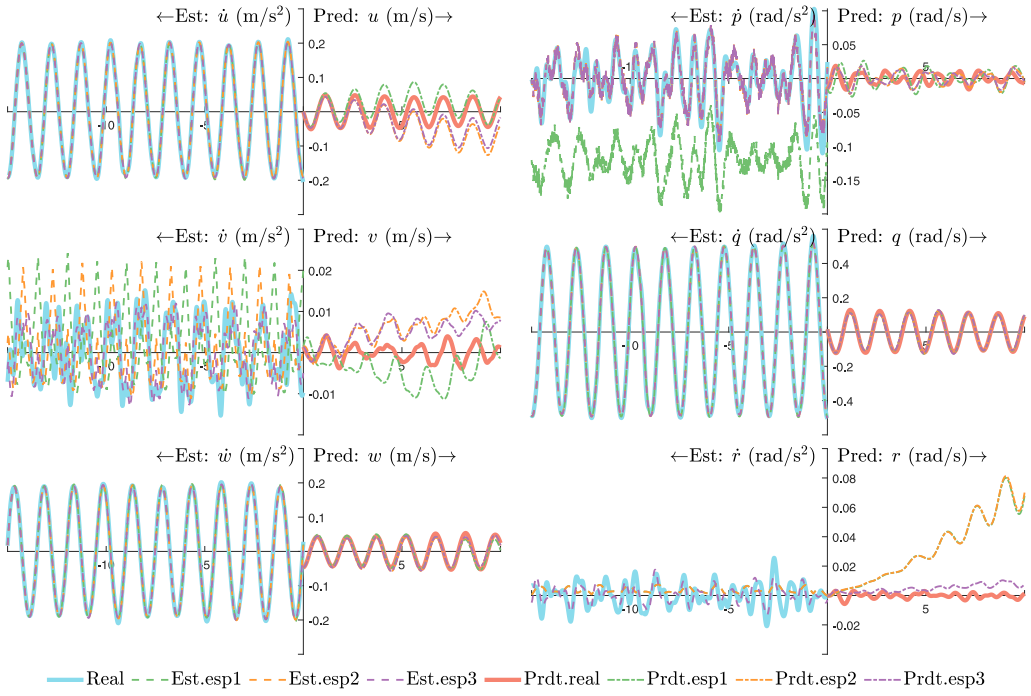

Fig. 3. Fitting of acceleration (left parts) and prediction of velocity (right parts) for $T_p = 1.5$ s and $\beta_w = 0$ deg.

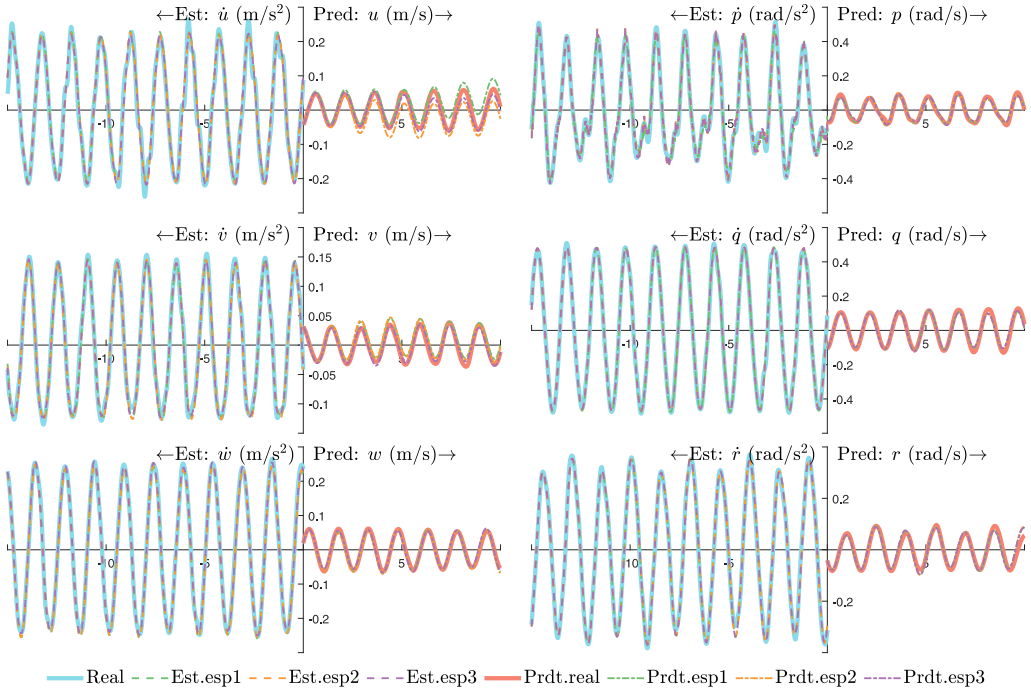

Fig. 4. Fitting of acceleration (left parts) and prediction of velocity (right parts) for $T_p = 1.5$ s and $\beta_w = 30$ deg.

A large number of candidate functions and sufficiently long measurement period ensure the model accuracy. However, the computation time increases in return. When the vessel is exposed to irregular waves, a growing amount of measurements are

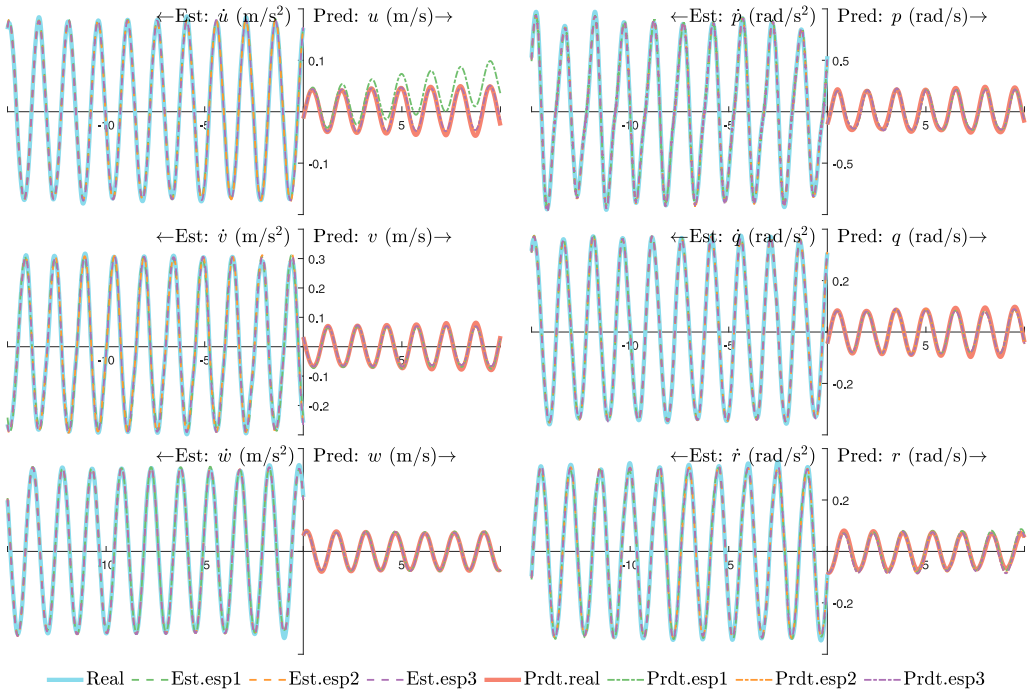

Fig. 5. Fitting of acceleration (left parts) and prediction of velocity (right parts) for $T_p = 1.5$ s and $\beta_w = 60$ deg.

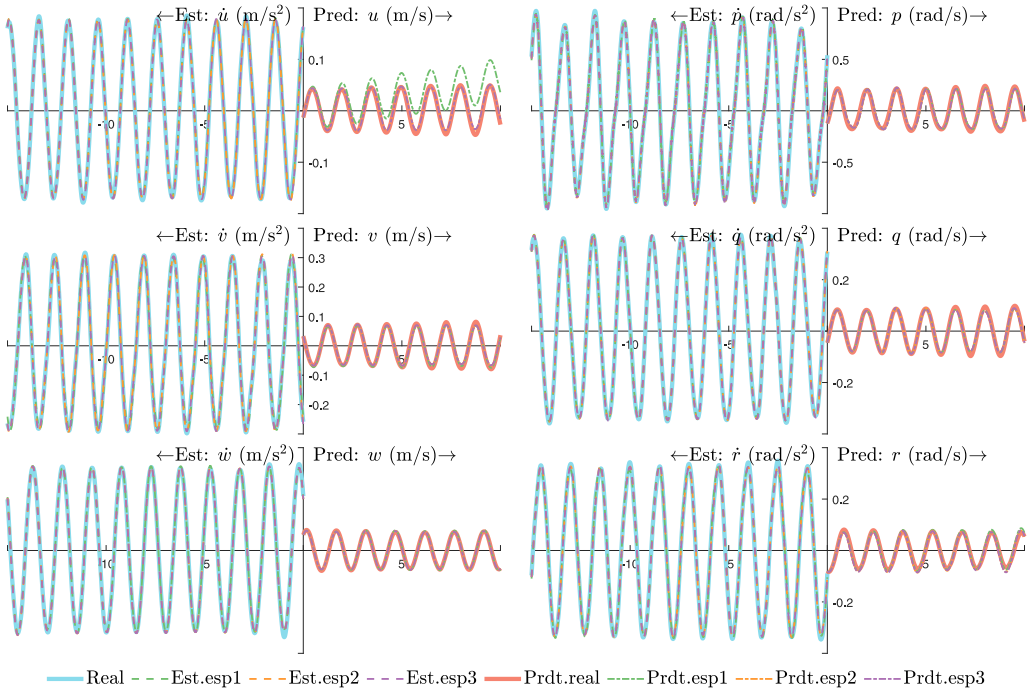

Fig. 6. Fitting of acceleration (left parts) and prediction of velocity (right parts) for $T_p = 1.5$ s and $\beta_w = 90$ deg.

required, which results in a longer calculation time. This is a weakness of the proposed algorithm. Moreover, the encounter frequency should be considered when the speed of advance changes. Since the added mass M_A is frequency-dependent, the added mass also changes with the speed of advance. Consequently, the number of unknown surges from $n_1 + n_2$ to $n_{\omega_e} \times (n_1 + n_2)$, where n_{ω_e} is

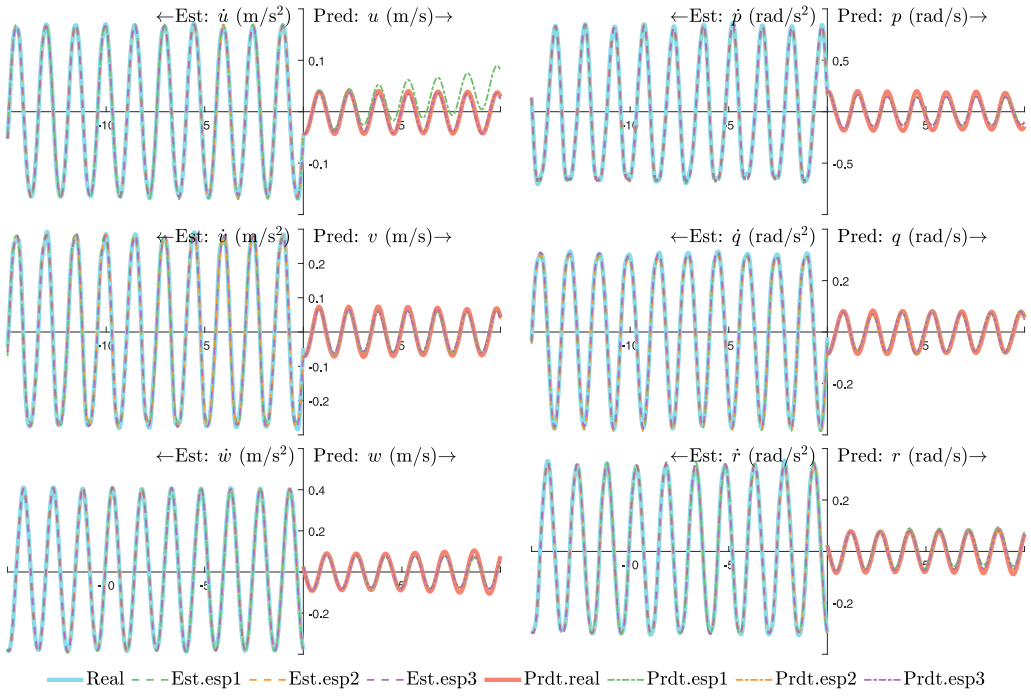

Fig. 7. Fitting of acceleration (left parts) and prediction of velocity (right parts) for T_p = 1.5 s and β_w = 120 deg.

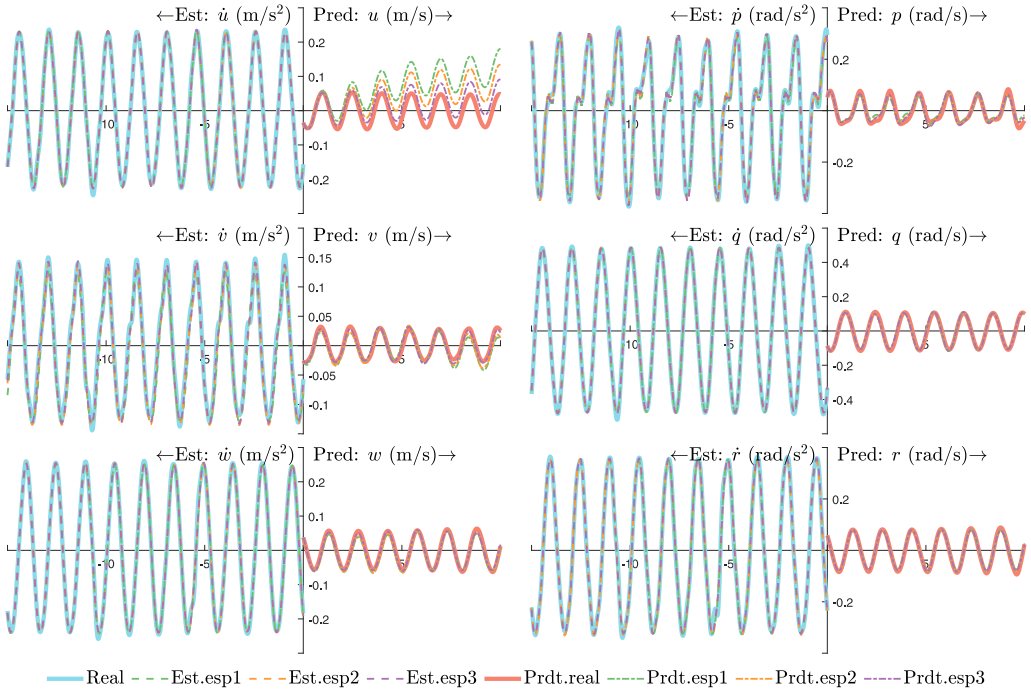

Fig. 8. Fitting of acceleration (left parts) and prediction of velocity (right parts) for T_p = 1.5 s and β_w = 150 deg.

the number of considered encounter frequencies. Such large amount of unknowns can cause problem to the calculation process. Therefore, a reasonable model complexity is the tradeoff of model accuracy and computational speed.

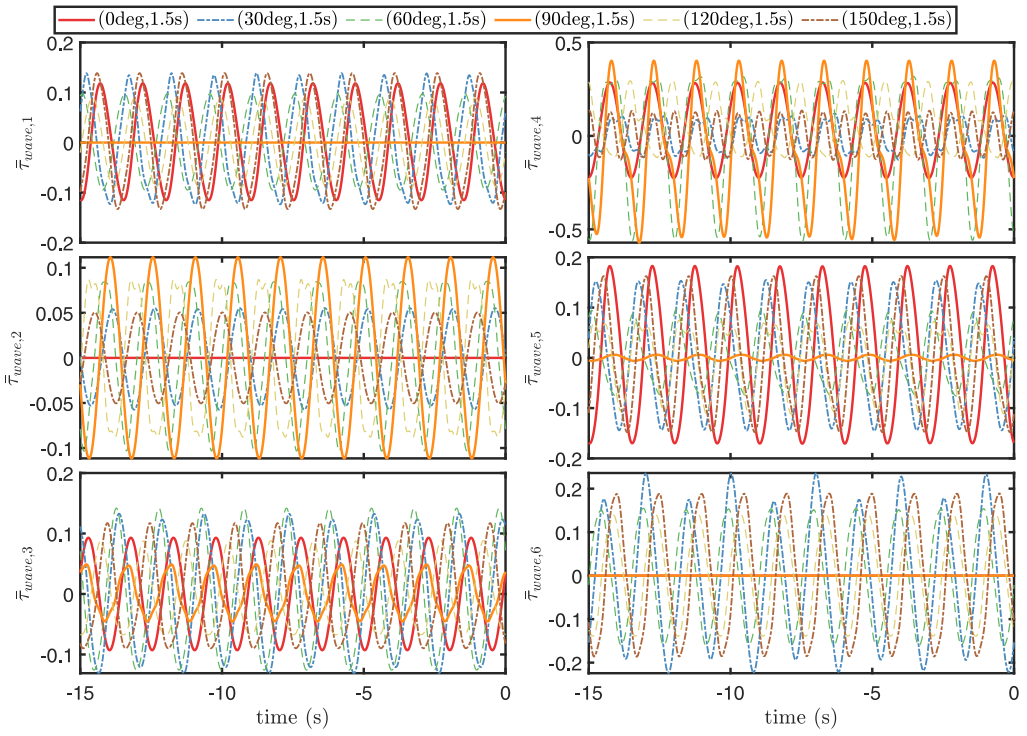

Fig. 9. Dimensionless wave-induced motion in 6 DOFs for $T_p = 1.5$ s and esp1.

4.3. Results: Wave load estimation

The fitting and prediction rely on the system dynamics and the identification of wave loads. The estimated dimensionless wave-induced loads with respect to headings are presented in Figs. 9–11. The legend is the vessel heading and period of the generated waves. Each line presents an individual test. Hence, there is no correlation among different lines in a same subplot.

It is impossible to directly verify the results since wave loads are not measurable. The RAOs and added mass are coupled. However, the results correlate to the wave generator, i.e., comparing the results for different incoming wave directions gives convincing proof.

The wave loads are harmonic which agrees with expectation. Moreover, the periods of the fitted wave loads in different DOFs are about 1.5 s, which is the same as the value of T_p set to the wave generator.

When $\beta_{wave} = 0$, the wave-induced force in the sway direction τ_{wave2} is almost zero. The same phenomenon was noticed for $\beta_{wave} = 90$ deg, i.e., the wave-induced force in the surge direction τ_{wave1} was close to zero.

Although the ship was not symmetric about the y^b-axis, the wave-induced loads with symmetric incoming wave directions about the y^b-axis could have a similar amplitude. This relationship is shown in the curves of $\beta_{wave} = 60$ deg and $\beta_{wave} = 120$ deg, and the curves of $\beta_{wave} = 30$ deg and $\beta_{wave} = 150$ deg.

Using the identified wave model, the vessel motion prediction is accurate. Therefore, we believe that the wave load estimation is reasonable. By comparing the three figures, it is noticed that the estimated wave loads are almost the same. Hence, the difference among the identified wave models with different thresholds is negligible.

4.4. Comparison with online estimation

To the best of our knowledge, this paper is the first work of white-box 6DOF vessel explicit model identification. It is difficult to select a counterpart since most research on 6DOF ship model identification is based on black-boxed learning methods. Therefore, we compared the results with a typical online estimation of the constant parameters of the linear regression [9,40], given by

$$\begin{bmatrix} \dot{\zeta} \\ \dot{\zeta}_w \end{bmatrix} = \Gamma \begin{bmatrix} \varphi(\eta, \nu, \tau_{thr}) \\ \varphi_w \end{bmatrix} (\dot{\nu} - \zeta^\top \varphi(\eta, \nu, \tau_{thr}) - \zeta_w^\top \varphi_w) \tag{14}$$

where $\Gamma \in \mathbb{R}^{(n_1+n_2)\times(n_1+n_2)}$ is the positive definite adaptation gain.

The same library of candidate functions was applied to achieve real-time estimation. The performance is shown in Fig. 12. Though the data fitting (in the left side) is acceptable, the motion prediction (in the left side) based on the identified model drift away, which indicates that the identified model cannot accurately present the system dynamics and environmental loads. Since the online estimation cannot fully utilize the historical data, the parameters oscillate with time; see Fig. 13 as an example.

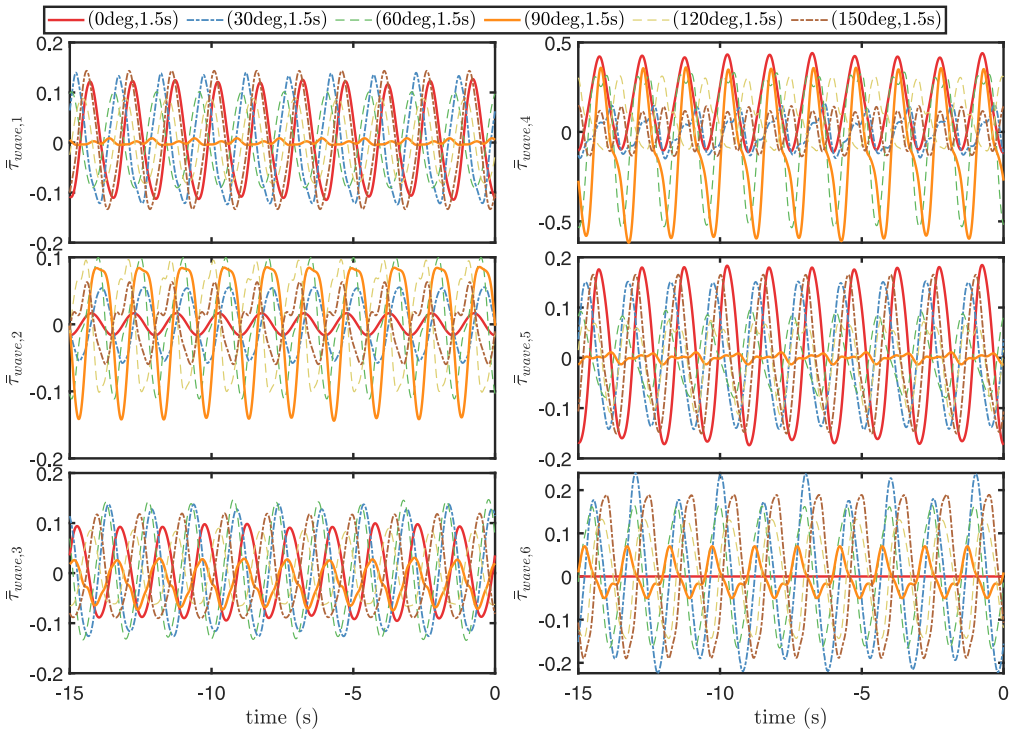

Fig. 10. Dimensionless wave-induced motion in 6 DOFs for $T_p = 1.5$ s and esp2.

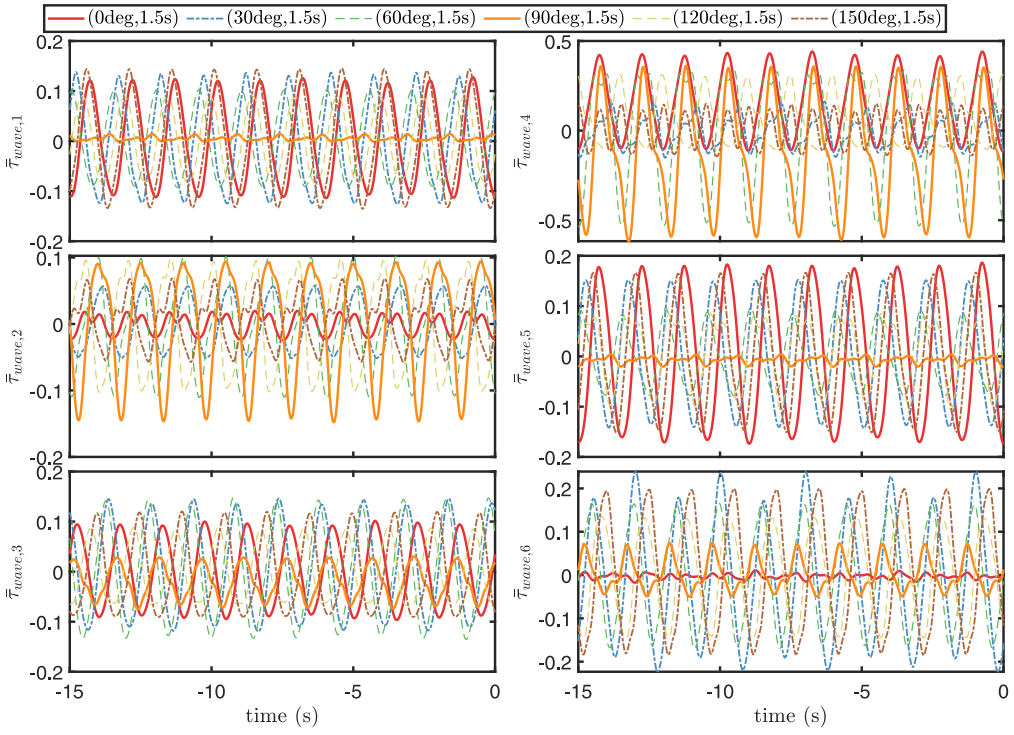

Fig. 11. Dimensionless wave-induced motion in 6 DOFs for $T_p = 1.5$ s and esp3.

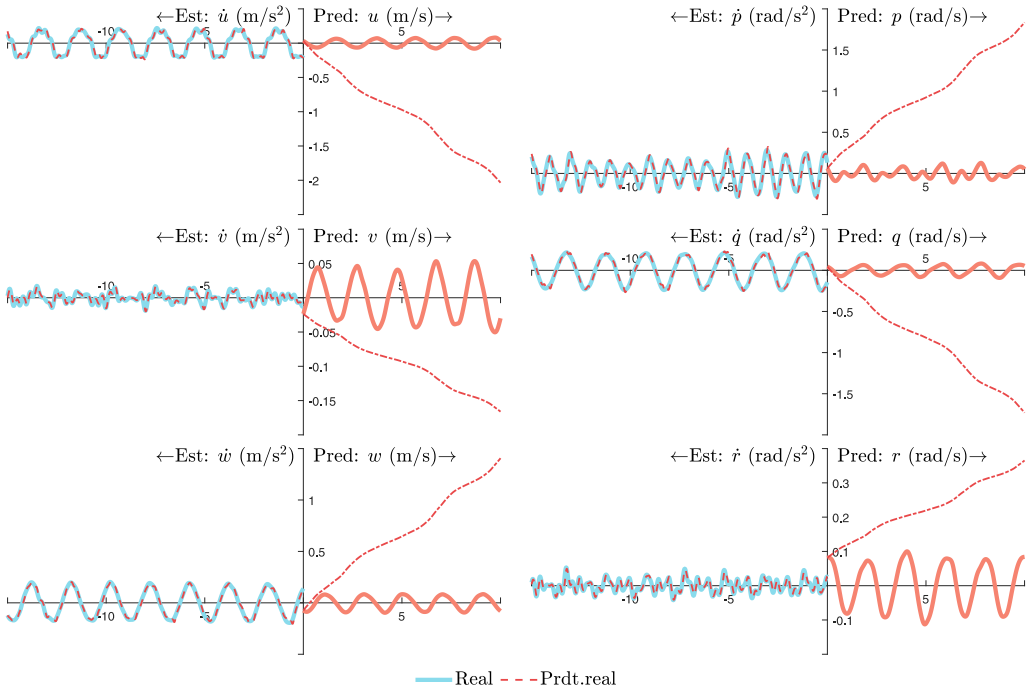

Fig. 12. Fitting of acceleration (left parts) and prediction of velocity (right parts) using online estimation for $T_p = 1.5$ s and $\beta_w = 30$ deg.

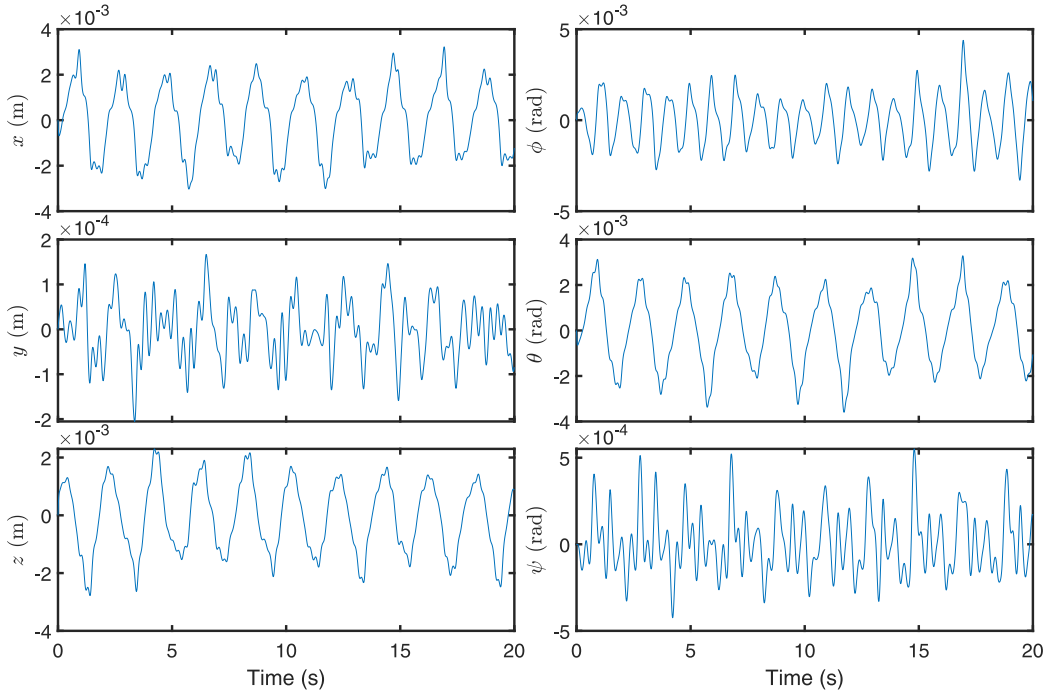

Fig. 13. The values of the third element in ζ for different DOFs.

5. Conclusions and future research

In this paper, a framework for data-driven 6DOF ship model identification based on ship motion measurements and the corresponding wave load estimation is proposed. The hydrodynamic coefficients, thruster input, mooring system, wind and wave excitation loads are considered in the model. Sparse regression is applied to fit the measurements. The algorithm was analyzed and verified through experiments. The reduced-order system extracts the main features of the system dynamics and guarantees the physical meaning of the candidate functions. It provides an opportunity to balance the model accuracy and complexity. A comparative study is undertaken to verify the proposed method. The proposed algorithm can be extended to other floating structures. Based on the identified model, short-term motion prediction can be achieved through direct integration. However, the computational speed should be improved remarkably before real-time applications.

Satisfactory identification comes from accurate real-time measurements. Future studies should attempt to improve the estimation accuracy and reduce the computation time. The model identification in more complicated scenarios, such as with time-varying speed and heading, is another future research target. In addition, we will further improve the robustness against noisy measurements when there are sensor noise and multi-source information.

Declaration of competing interest

The authors declare that they have no known competing financial interests or personal relationships that could have appeared to influence the work reported in this paper.

Acknowledgments

This work was supported by the Research Council of Norway (RCN) through the Centre for Research-based Innovation on Marine Operations (SFI MOVE, RCN-project 237929) and the Centre of Excellence on Autonomous Marine Operations and Systems (NTNU AMOS, RCN-project 223254), and partially supported by the National Natural Science Foundation of China (Grant No. 52071058).

References

[1] Y. Ren, V. Venugopal, W. Shi, Dynamic analysis of a multi-column TLP floating offshore wind turbine with tendon failure scenarios, Ocean Eng. 245 (2022) 110472.
[2] W. Hu, T. Zhang, X. Deng, Z. Liu, J. Tan, Digital twin: A state-of-the-art review of its enabling technologies, applications and challenges, J. Intell. Manuf. Special Equip. (2021).
[3] H. Niu, Z. Ji, A. Savvaris, A. Tsourdos, Energy efficient path planning for unmanned surface vehicle in spatially-temporally variant environment, Ocean Eng. 196 (2020) 106766.
[4] B. Wu, G. Li, L. Zhao, H.-I.J. Aandahl, H.P. Hildre, H. Zhang, Navigating patterns analysis for onboard guidance support in crossing collision-avoidance operations, IEEE Intell. Transp. Syst. Magaz. (2021) 2–17.
[5] M.H. Casado, R. Ferreiro, Identification of the nonlinear ship model parameters based on the turning test trial and the backstepping procedure, Ocean Eng. 32 (11–12) (2005) 1350–1369.
[6] X.-R. Hou, Z.-J. Zou, C. Liu, Nonparametric identification of nonlinear ship roll motion by using the motion response in irregular waves, Appl. Ocean Res. 73 (2018) 88–99.
[7] X. Han, B.J. Leira, S. Sævik, Vessel hydrodynamic model tuning by discrete Bayesian updating using simulated onboard sensor data, Ocean Eng. (2021) 108407.
[8] K.J. Åström, C.G. Källström, Identification of ship steering dynamics, Automatica 12 (1) (1976) 9–22.
[9] R. Skjetne, Ø.N. Smogeli, T.I. Fossen, A nonlinear ship manoeuvering model: Identification and adaptive control with experiments for a model ship, 2004.
[10] S. Sutulo, C.G. Soares, An algorithm for offline identification of ship manoeuvring mathematical models from free-running tests, Ocean Eng. 79 (2014) 10–25.
[11] G. Rajesh, S. Bhattacharyya, System identification for nonlinear maneuvering of large tankers using artificial neural network, Appl. Ocean Res. 30 (4) (2008) 256–263.
[12] G. Xia, J. Liu, X. Chen, D. Wang, R. Yang, EKF based model identification for a relaxed dynamic positioning ship using NMPC method, in: 2015 IEEE Inter Conference on Mechatronics and Automation (ICMA), IEEE, 2015, pp. 1313–1318.
[13] S.-L. Dai, C. Wang, F. Luo, Identification and learning control of ocean surface ship using neural networks, IEEE Trans. Ind. Inf. 8 (4) (2012) 801–810.
[14] Z. Wang, Z. Zou, C.G. Soares, Identification of ship manoeuvring motion based on nu-support vector machine, Ocean Eng. 183 (2019) 270–281.
[15] G. Xia, A. Zhao, X. Chen, G. Wang, Nonlinear model identification of a ship using recursive subspace methods, in: 2015 IEEE International Conference on Mechatronics and Automation (ICMA), IEEE, 2015, pp. 1385–1390.
[16] S. Xie, X. Chu, C. Liu, J. Liu, J. Mou, Parameter identification of ship motion model based on multi-innovation methods, J. Mar. Sci. Technol. 25 (1) (2020) 162–184.
[17] B. Mei, L. Sun, G. Shi, White-black-box hybrid model identification based on RM-RF for ship maneuvering, IEEE Access 7 (2019) 57691–57705.
[18] H. Zhou, Z. Ren, M. Marley, R. Skjetne, A guidance and maneuvering control system design with anti-collision using stream functions with vortex flows for autonomous marine vessels, IEEE Trans. Control Syst. Technol. (2022) 1–16.
[19] S.A. Værnø, R. Skjetne, Ø.K. Kjerstad, V. Calabrò, Comparison of control design models and observers for dynamic positioning of surface vessels, Control Eng. Pract. 85 (2019) 235–245.
[20] S. Sutulo, C.G. Soares, Synthesis of experimental designs of maneuvering captive-model tests with a large number of factors, J. Mar. Sci. Technol. 9 (1) (2004) 32–42.
[21] T. Wang, G. Li, B. Wu, V. Æsøy, H. Zhang, Parameter identification of ship manoeuvring model under disturbance using support vector machine method, Ships Offshore Struct. (2021) 1–9.
[22] M. Zhu, A. Hahn, Y. Wen, A. Bolles, Parameter identification of ship maneuvering models using recursive least square method based on support vector machines, TransNav: Int. J. Mar. Navig. Saf. Sea Transp. 11 (2017).
[23] K.J. Astrom, C. Kallstrom, N. Norrbin, L. Bystrom, The identification of linear ship steering dynamics using maximum likelihood parameter estimation, 1975.

[24] T. Wang, G. Li, L.I. Hatledal, R. Skulstad, V. sy, H. Zhang, Incorporating approximate dynamics into data-driven calibrator: A representative model for ship maneuvering prediction, IEEE Trans. Ind. Inf. (2021) 1.
[25] M.R. Haddara, J. Xu, On the identification of ship coupled heave–pitch motions using neural networks, Ocean Eng. 26 (5) (1998) 381–400.
[26] M. Araki, H. Sadat-Hosseini, Y. Sanada, K. Tanimoto, N. Umeda, F. Stern, Estimating maneuvering coefficients using system identification methods with experimental, system-based, and CFD free-running trial data, Ocean Eng. 51 (2012) 63–84.
[27] N.K. Kumar, R. Savitha, A. Al Mamun, Ocean wave characteristics prediction and its load estimation on marine structures: A transfer learning approach, Mar. Struct. 61 (2018) 202–219.
[28] O. Faltinsen, Sea Loads on Ships and Offshore Structures, Vol. 1, Cambridge University Press, 1993.
[29] J.N. Newman, P. Sclavounos, The unified theory of ship motions, Technical Report, Massachusetts Inst of Tech Cambridge Dept of Ocean Engineering, 1980.
[30] G.E. Hearn, Alternative methods of evaluating Green's function in three-dimensional ship-wave problems, J. Ship Res. 21 (2) (1977).
[31] D.C. Kring, Time domain ship motions by a three-dimensional Rankine panel method, (Ph.D. thesis), Massachusetts institute of technology, 1994.
[32] S.L. Brunton, J.L. Proctor, J.N. Kutz, Discovering governing equations from data by sparse identification of nonlinear dynamical systems, Proc. Natl. Acad. Sci. 113 (15) (2016) 3932–3937.
[33] Z. Ren, X. Han, A.S. Verma, J.A. Dirdal, R. Skjetne, Sea state estimation based on vessel motion responses: Improved smoothness and robustness using Bézier surface and L1 optimization, Mar. Struct. 76 (2021) 102904.
[34] X. Cheng, G. Li, P. Han, R. Skulstad, S. Chen, H. Zhang, Data-driven modeling for transferable sea state estimation between marine systems, IEEE Trans. Intell. Transp. Syst. 23 (3) (2022) 2561–2571.
[35] R. Skjetne, Z. Ren, A survey on modeling and control of thruster-assisted position mooring systems, Mar. Struct. 74 (2020) 102830.
[36] W. Deng, Z. Li, X. Li, H. Chen, H. Zhao, Compound fault diagnosis using optimized MCKD and sparse representation for rolling bearings, IEEE Trans. Instrum. Meas. (2022).
[37] W. Deng, J. Xu, X.-Z. Gao, H. Zhao, An enhanced MSIQDE algorithm with novel multiple strategies for global optimization problems, IEEE Trans. Syst. Man Cybern. (2022).
[38] G. Udjus, Force field identification and positioning control of an autonomous vessel using inertial measurement units, (Master's thesis), NTNU, 2017.
[39] J. Bjørnø, Thruster-assisted position mooring of C/S inocean cat i drillship, (Master's thesis), NTNU, 2016.
[40] R. Ortega, L. Praly, S. Aranovskiy, B. Yi, W. Zhang, On dynamic regressor extension and mixing parameter estimators: Two luenberger observers interpretations, Automatica 95 (2018) 548–551.